JOURNAL OF PROPULSION AND POWER
Vol. 22, No. 5, September–October 2006

Endurance Test of Microwave Engine

S.-W. Kim,* H. Okamoto†, and T. M. Sugiki‡
Astro Research Corporation, Kanagawa 240-0005, Japan
Y. Itoh§
ULVAC, Inc., Kanagawa 253-8543, Japan
S. Satori¶
Hokkaido Institute of Technology, Hokkaido 006-8585, Japan
and
M.-R. Nam**
Korea Advanced Institute of Science and Technology, Daejeon 305-701, Republic of Korea

A low-power, microwave-discharge-type electrostatic thruster has been developed for 50 kg-class microsatellites. A breadboard model of the microwave engine was manufactured, and two endurance tests were performed to verify its durability. During the first endurance test of 1200 h, only slight changes in the thruster discharge chamber were observed. However, the stainless-steel magnetic nozzle just downstream of the discharge chamber had sputter damage near the nozzle exit extending to the midsection of the Sm-Co magnets on the inner wall. Although the thruster operation was unaltered by the sputter damage, it was decided to shield the magnetic nozzle surface with graphite to protect it from impinging ions and reduce sputtering. Thus, the magnetic nozzle was replaced by one with a graphite shield for the second endurance test. Also, the filament neutralizer was replaced by a microwave-discharge neutralizer. The thruster discharge chamber, including the antenna, was kept from the first endurance test. After more than 5000 h of operation in the second endurance test, thruster operation became unstable, and the endurance test was stopped. The microwave neutralizer had logged over 5500 h of operation. The magnetic nozzle with a graphite shield had logged over 5200 h of operation. The other parts of the thruster had logged over 7100 h of operation.

Nomenclature

e = elementary charge
g_0 = acceleration of gravity
I_{ac} = acceleration current
I_b = beam current
I_{sp} = specific impulse
M_i = ion mass of Xenon
$\dot{m}_i$ = ion mass flow rate exiting the thruster as ion beam
$\dot{m}_p$ = Xenon propellant flow rate
P_{tot} = total system power
P_μ = total microwave power
T = thrust
u_i = ion speed
V_{ac} = acceleration voltage
η_{ac} = acceleration efficiency
η_T = total thrust efficiency
η_u = propellant utilization efficiency
θ_{div} = beam divergence half-angle

Presented as Paper 2004-4126 at the AIAA/ASME/SAE/ASEE 40th Joint Propulsion Conference and Exhibit, Fort Lauderdale Florida, 11–14 July 2004; received 18 April 2005; revision received 22 November 2005; accepted for publication 5 January 2006.

*Senior Engineer, Space Systems Division, 134 Godo-cho Hodogaya-ku, Yokohama. Member AIAA.
†Manager, Space Systems Division, 134 Godo-cho Hodogaya-ku, Yokohama.
‡President, 134 Godo-cho Hodogaya-ku, Yokohama. Member AIAA Technical Committee.
§Engineer, Flat Panel Display Equipment Group, 2500 Hagisono, Chigasaki.
¶Associate Professor, Hokkaido Institute of Technology, Department of Electrical and Electronic Engineering, Maeda7jo Teine-ku. Member AIAA.
**Research Professor, Satellite Technology Research Center, 373-1, Guseong-dong, Yuseong-gu.

I. Introduction

THE microwave engine is a low-power, microwave-discharge electrostatic thruster that is well suited for 50-kg-class microsatellites. Until now, microsatellites have had only limited maneuvering capability because of power and mass constraints. The 30-W, compact microwave engine allows microsatellites to utilize a high-I_{sp} thruster system for orbit transfer and attitude control. For example, microsatellites are usually launched as secondary payloads and are often released in orbits that are suboptimal for their missions. In such cases, a microwave engine can transfer the microsatellite to an optimal orbit. Another role for the microwave engine is atmospheric drag compensation in the low Earth orbit (LEO). By having the microwave engine onboard, microsatellites can operate in LEO longer. This capability is particularly advantageous for remote sensing applications because high-resolution images can be obtained by relatively inexpensive microsatellites from LEO without new advances in sensor technologies. The microwave engine enhances functionality and lifetime of microsatellites, thus expanding their utility for a number of space applications. The miniature microwave thruster can provide stationkeeping and primary propulsion solutions for the microsatellites. The priority in the development of the microwave engine was placed upon minimizing the total system power, sacrificing thrust and efficiency to a certain degree. The target for total system power was set to 30 W. This approach was chosen because of the very limited power onboard most microsatellites.

II. Experimental Setup

A. Facility

Experiments were conducted in a 0.5-m-long by 0.15-m-diam glass vacuum chamber with a 0.15-m-diam port at the midsection for pumping. The glass chamber was pumped by a 22-cm-diam TOKUDA ESV-8 oil diffusion pump backed by an ALCATEL PASCAL 2021 I rotary pump for a xenon (Xe) pumping speed

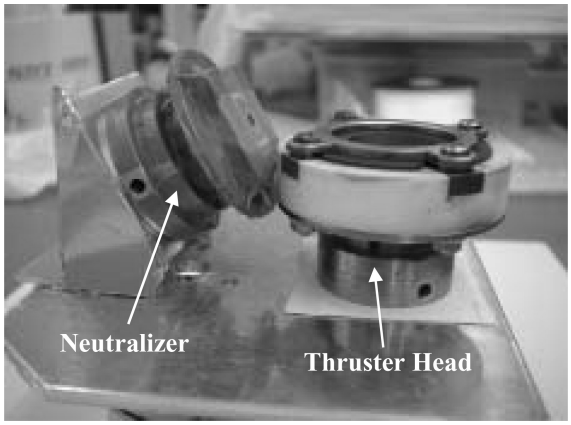

Fig. 1 Picture of the breadboard model microwave engine.

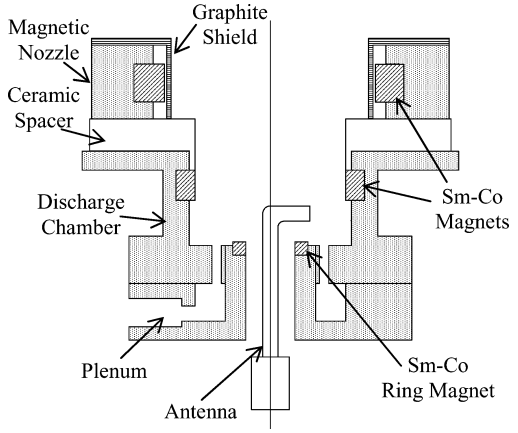

Fig. 2 Detailed schematic of the microwave engine discharge chamber and magnetic nozzle. The Sm-Co magnets in the discharge chamber form ECR regions where primary ionization occurs. The ECR formation is influenced by the Sm-Co magnets in the magnetic nozzle.

of approximately 1500 L/s. During thruster operation, the background pressure was approximately 2.6×10^{-3} Pa (2.0×10^{-5} torr) (corrected for xenon) and was measured by a UNITEC IG-8 hot-cathode ionization gauge. The gauge was located on a vacuum port just above the diffusion pump. The chamber base pressure was roughly 4×10^{-4} Pa (3×10^{-6} torr) (air) for these tests. High-purity (99.995% pure) xenon propellant was supplied to the microwave engine from a compressed gas bottle through stainless-steel feed lines. Propellant flows to the thruster discharge chamber and neutralizer were controlled and monitored with separate STEC SEC-7320R mass flow controllers specifically calibrated for xenon. The system is capable of providing up to 0.1 mg/s of xenon with an accuracy of within 1% of the full-scale value, according to the manufacturer.

B. Microwave Engine

Figure 1 shows a picture of the breadboard model microwave engine, and Fig. 2 shows a detailed schematic of the microwave engine discharge chamber and magnetic nozzle.

The microwave engine consists of four major components: discharge chamber, magnetic nozzle, neutralizer, and ignitor. The microwave engine utilizes 1.5-GHz microwave power to heat the electrons, resulting in excitation and ionization of Xe propellant by electron impacts in the discharge chamber. The Sm-Co magnets in the discharge chamber form electron cyclotron resonance (ECR) regions where electrons resonantly absorb energy from the microwave. Primary ionization occurs in the ECR region. Then, hot electrons in the ECR region diffuse into the bulk of the plasma and excite/ionize neutrals there. Unabsorbed microwave power is converted to other modes by scattering (wave vector change), and then, is more or less absorbable via the resonance modes.[1] Microwave

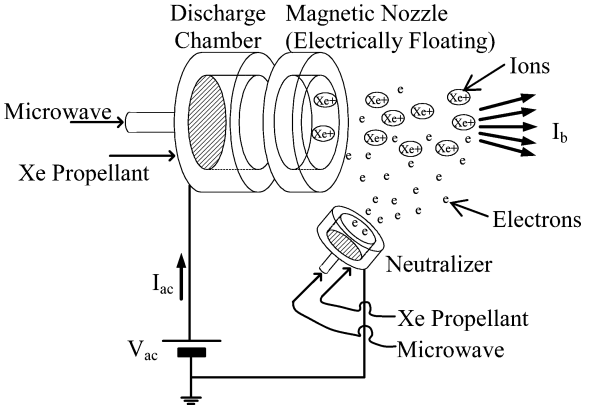

Fig. 3 Simple electrical schematic of the microwave engine indicating the acceleration current I_{ac} and the beam current I_b.

power is transmitted to the plasma by a KAMAN Instrumentation's ultra-high-vacuum microwave feed-through (part # 853872). The molybdenum antenna is at the discharge chamber potential to reduce sputtering.

The role of the magnetic nozzle is to minimize the likelihood of forming a dc (glow) discharge between the neutralizer and the discharge chamber and to facilitate microwave discharge. As indicated in Fig. 3, the beam current I_b is the ion beam current that exits the thruster and generates thrust. The acceleration current I_{ac} is the current supplied by the acceleration voltage power supply. The difference between I_{ac} and I_b is the electron current caused by electrons from the neutralizer that enter the discharge chamber. This electron current is a loss mechanism and should be minimized. Therefore, a magnetic nozzle is placed downstream of the discharge chamber to form a magnetic field that suppresses the axial mobility of electrons from the neutralizer. The magnetic nozzle is electrically floating with a ceramic spacer between the discharge chamber and the magnetic nozzle (Fig. 2).

The neutralizer has the same basic configuration as the discharge chamber. It also utilizes 1.5-GHz microwave and ECR condition to generate plasma. However, the positions and dimensions of the antenna and Sm-Co magnets are modified to optimize electron emission. In addition, the neutralizer has an orifice at the exit instead of a ceramic spacer and magnetic nozzle. The neutralizer is at ground potential and does not have an extraction electrode. Electrons are extracted from the orifice by the potential gradient between the plasma plume and the neutralizer. The antenna is electrically shorted to the neutralizer body.

The ignitor is a rhenium-tungsten wire loop inserted in the discharge chamber. After the Xe propellant flow and microwave power to the discharge chamber are supplied, the ignitor is turned on by flowing 5 A of current for 0.35 s. When enough thermal electrons are emitted from the ignitor surface, plasma is ignited after which the ignitor is shorted to the discharge chamber by a switch in order to minimize sputtering. At this point, the propellant flow and microwave power to the neutralizer are supplied, and the acceleration voltage is turned on. Occasional ion impingements on the neutralizer walls induce secondary electrons that ignite the neutralizer plasma.

Ions in the discharge chamber drift along the thruster axis primarily by the pressure gradient until a fraction of them reaches the ceramic spacer region where the ions start to experience a voltage gradient between the discharge chamber at the acceleration voltage of 250 V and the neutralizer at ground potential. (Fig. 3) There is no electrode downstream to extract ions. Therefore, the beam current is not limited by the space charge limitation. The microwave engine is basically a two-stage electric propulsion thruster where ionization and acceleration occur in separate regions. Some ionization, however, occurs downstream of the discharge chamber that contributes to ion energy broadening and ion beam divergence. The potential of the magnetic nozzle is approximately 70 V above ground when V_{ac} is +250 V with respect to ground.

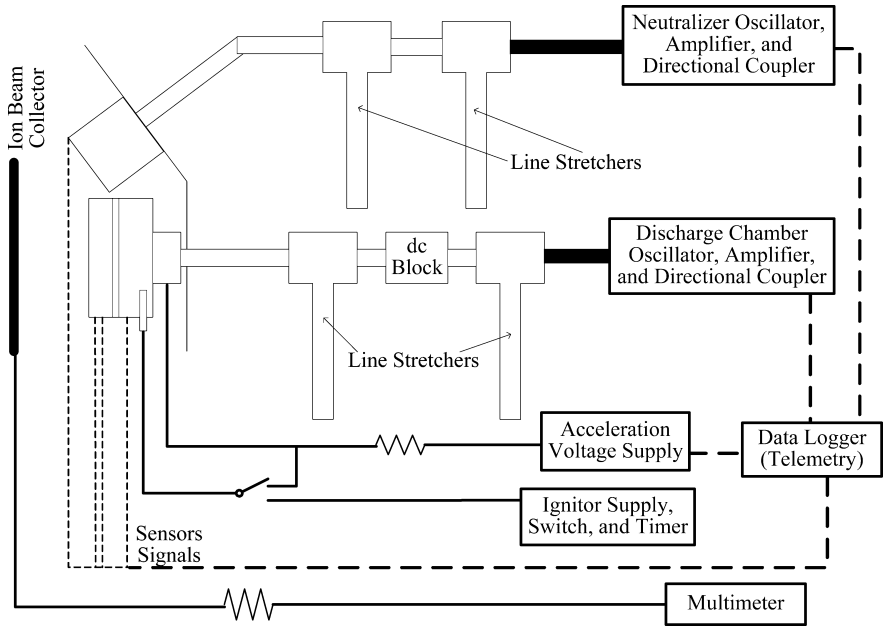

Fig. 4 Block diagram of the microwave engine system. (Propellant supply system not included.)

C. Experimental Measurements

A block diagram of the microwave engine system (excluding propellant supply system) is shown in Fig. 4. The 1.5-GHz microwave oscillator-amplifier-directional coupler assemblies were custom-built by Milli Com Corporation in Osaka, Japan. These assemblies have variable attenuators to adjust output power from the maximum of 10 W. Hirose coaxial line stretchers (model HLS-JJ-1) were placed between the microwave generators and plasma sources to prevent the high reflection of microwave power as a result of a mismatch of the plasma impedance. Once the impedance was matched, few adjustments were needed. The ends of the line stretchers were shorted terminators in order to have the antenna at the same potential as the discharge chamber or the neutralizer body. A dc block was inserted between the two line stretchers in the discharge chamber microwave coaxial line so that the portion of the coaxial line leading up to the antenna was held at the acceleration potential.

The acceleration voltage was supplied by a TAKASAGO GPO500-1R (500 V/1 A) power supply. The ignitor current was supplied by a LAMBDA PWS-350-10 (10 V/35 A) power supply. The ignitor timer and switch were manufactured in house. National Semiconductor's LM35DZ IC temperature sensors were attached to the discharge chamber, magnetic nozzle, neutralizer, and microwave amplifiers to measure their temperatures. The accuracy of the temperature measurements was $\pm 1^{\circ}$C according to the manufacture. Microwave forward and reflected power was measured using diode detectors built and calibrated in house. Acceleration current was measured by a 10-Ω shunt resistor. Acceleration voltage and magnetic nozzle potential were measured using voltage dividers built in house. The voltage signals from diode detectors, voltage dividers, I_{ac} shunt resistor, and temperature sensors were measured and stored by a NEC OMNIACE RT3600 data logger. The measured values had accuracy within $\pm 1\%$ of the true value.

Beam current was measured by a 10-Ω shunt resistor. The ion beam collector in Fig. 4 was actually a stainless-steel cylinder. The cylinder covered most of the inner wall of the glass chamber, except the pumping port at the midsection where a stainless-steel mesh was used to collect ions. The ion beam collector was biased -25 V with respect to ground to repel electrons. The voltage signal from the I_b shunt resistor was measured using a FLUKE 73III multimeter that had a measurement accuracy of within 1% of the true value. A MAGNA MG-401 gauss meter and a MG-401PRB probe were used to measure magnetic flux densities in these tests to within 5 G of accuracy. Mass measurements in these tests used an A&D GX-200 electronic balance that had accuracy of ± 0.002 g. Dimensions in these tests were measured using a micrometer caliper with an accuracy of ± 0.03 mm.

D. Thruster Performance

The microwave engine performance tests have been performed, and the results have been reported in previous papers.[2–7] Normal operating parameters of the microwave engine were the following: 1) discharge chamber propellant flow 0.038 mg/s (0.42 SCCM), 2) neutralizer propellant flow 0.022 mg/s (0.25 SCCM), 3) discharge microwave input power 5.0 W, 4) neutralizer microwave input power 2.4 W, and 5) acceleration voltage 250 V.

Typical numbers of the experimental measurements for the preceding operating condition were the following: discharge microwave reflected power 0.3 W, neutralizer microwave reflected power 0.1 W, acceleration current 43.0 mA, beam current 27.6 mA, magnetic nozzle potential 70 V, discharge chamber temperature 68°C, magnetic nozzle temperature 75°C, and neutralizer temperature 76°C. As mentioned in the preceding subsection describing the microwave engine, the difference between I_{ac} and I_b is a loss mechanism that does not contribute to thrust, and thus the acceleration efficiency is defined to represent this loss as follows:

$$\eta_{ac} = I_b / I_{ac} \tag{1}$$

In the thruster performance calculations, P_μ is the sum of the discharge microwave power and neutralizer microwave power. Also, $\dot{m}_p$ is the sum of the discharge chamber and neutralizer propellant flows. All beam ions were assumed to be singly ionized. Although the double-to-single ion current ratio was not measured, it was thought to be very small because the microwave powers and propellant flows were set as low as possible for a stable thruster operation in order to minimize total system power P_{tot}.

The total system power P_{tot} is the sum of the microwave power P_μ and acceleration power $(V_{ac} \cdot I_{ac})$. However, the power losses caused by the microwave amplifier (50% efficiency, measured), microwave coaxial line transmission (78% efficiency, measured), and acceleration power supply (91% efficiency, quoted value) were included in the actual calculation of P_{tot}. Thus, $P_{tot} = (5.0 + 2.4)/(0.5 * 0.78) + (0.043 * 250)/0.91 = 30.8$ W.

Propellant utilization efficiency is defined as the ratio of the thrust-generating ions to the propellant atoms supplied to the thruster and

Table 1 Typical microwave engine performance

Item	Value
Discharge chamber propellant flow rate (xenon)	0.038 mg/s
Neutralizer propellant flow rate (xenon)	0.022 mg/s
Discharge microwave power	5.0 W
Neutralizer microwave power	2.4 W
Acceleration voltage V_{ac}	250 V
Total system power P_{tot}	30.8 W
Acceleration current I_{ac}	43.0 mA
Beam current I_b	27.6 mA
Acceleration efficiency η_{ac}	0.64
Propellant utilization efficiency η_u	0.63
Thrust (calculated) T	0.6 mN
I_{sp}	1015 s
Total thrust efficiency η_T	0.15

can be expressed as the following:

$$\eta_u \equiv \dot{m}_i/\dot{m}_p = (M_i \cdot I_b)/(e \cdot \dot{m}_p) \tag{2}$$

Thrust was calculated by assuming that ionization and acceleration occur in completely separate regions and that all ions are accelerated by V_{ac}. Also, beam divergence half-angle was set to 34 deg from visual observation. Then, the thrust can be estimated using the following:

$$T = \dot{m}_i \cdot u_i = \sqrt{(2M_i/e)} \cdot \cos\theta_{div} \cdot I_b \cdot \sqrt{V_{ac}} \tag{3}$$

Specific impulse I_{sp} can be calculated from the thrust using its definition, $I_{sp} = T/(\dot{m}_p \cdot g_0)$. Total thrust efficiency is defined as the ratio of thrust power to total electrical power P_{tot} and can be calculated using the following:

$$\eta_T = \frac{\frac{1}{2}\dot{m}_i \cdot u_i^2}{P_{tot}} = \frac{1}{2}\frac{T \cdot I_{sp} \cdot g_0}{\eta_u \cdot P_{tot}} \tag{4}$$

Typical thruster performance numbers were calculated using the preceding equations and are summarized in Table 1. By the measurement accuracies described in the preceding subsection, the uncertainties for the thruster performance numbers were estimated to be within 5%. Here η_u and I_{sp} will greatly improve if a propellantless electron source such as a barium-impregnated cathode is used as a neutralizer. Such a neutralizer will also improve η_T because the required cathode heater power is much less than that needed for the neutralizer microwave power of more than 6 W (including amplifier and transmission line losses).

III. 1200-h Endurance Test

A breadboard model of the microwave engine was put through a preliminary endurance test of 1200 h to verify the durability of the thruster design before the 5300-h life test. The mass, dimensions, and magnetic flux densities of each part were measured before the test for later comparison. The neutralizer used in this first endurance test was a rhenium-tungsten filament neutralizer with triple carbonates [(Ba-Sr-Ca)CO_3] applied in and around the filament. It was decided to test the thruster head (discharge chamber and magnetic nozzle) first in the preliminary endurance test while a microwave neutralizer was being developed in order to make effective use of time. The microwave engine was disassembled after the 1200-h test, and the masses, dimensions, and magnetic flux densities were measured after each part was cooled down to room temperature.

Figure 5 shows a picture of the discharge chamber after 1200 h of operation. No significant sputtering could be observed inside the discharge chamber. The midsection of the Sm-Co permanent magnets on the inner wall of the discharge chamber became somewhat glossy. These surfaces appeared to be polished by the impinging ions with energies equivalent to the plasma potential. However, the ions were not expected to cause any significant damage because of their low energies. The magnetic flux density in the discharge chamber had, on average, decreased by 3.3%. There was virtually no deposition of sputtered material inside the discharge chamber.

Fig. 5 Discharge chamber after the 1200-h preliminary endurance test. No significant sputtering damage or deposition of sputtered material inside the discharge chamber. (The hole under the Sm-Co magnets on the inner wall is for installing a plasma ignitor.)

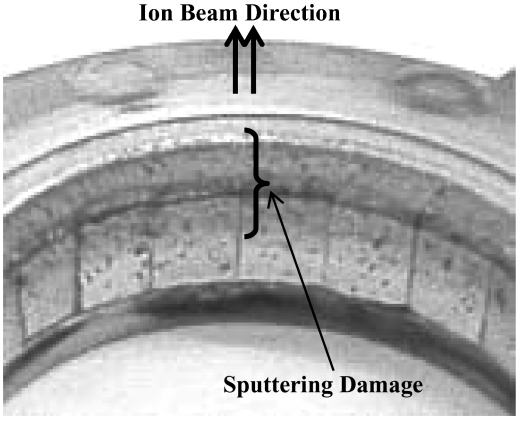

Fig. 6 Inner wall of the magnetic nozzle after the 1200-h preliminary endurance test. Sputtering damage can be seen near its exit (top) that extends to the midsection of the Sm-Co magnets on its inner wall.

The L-shaped, molybdenum antenna had a matte finish originally. But the antenna became glossy where it was exposed to the plasma. The polishing was also attributed to the ion impingements upon the antenna surface with the energies close to the plasma potential. The mass of the antenna decreased by 8.90 mg over the 1200 h. The diameter of the antenna decreased from 1.57 to 1.45 mm in the middle of the bent section. However, the diameter was the largest at the tip and decreased towards the bend. According to this rate of sputtering, the antenna diameter after 5000 h of thruster operation would be approximately 1 mm, and the antenna was expected to function normally.

Figure 6 shows a picture of the magnetic nozzle after 1200 h of operation. The magnetic nozzle had sputtering damage near its exit that extended to the midsection of the Sm-Co magnets on its inner wall. The diameter of the nozzle exit increased from 21.0 to 21.7 mm. The mass of the magnetic nozzle decreased by 466 mg. Deposition of metallic material was observed on the vacuum chamber wall that was thought to have come from the sputtered material from the magnetic nozzle. From the relative positions of the deposition and the magnetic nozzle exit, most of the sputtered material seemed to be confined within a half-angle of 35 deg with respect to the thruster axis. Magnetic flux density in the magnetic nozzle had decreased by 4.7% on average.

In general, magnetic flux density of a permanent magnet decreases as its temperature increases and vice versa. If the temperature reaches above a critical temperature, magnetic flux density cannot recover completely even after the magnet cools down. This critical temperature for Sm-Co magnets is 250°C according to the manufacture. The Sm-Co magnets in the microwave engine reached near 80°C, well below the critical temperature. Therefore, the decrease in magnetic flux density cannot be attributed to the operating

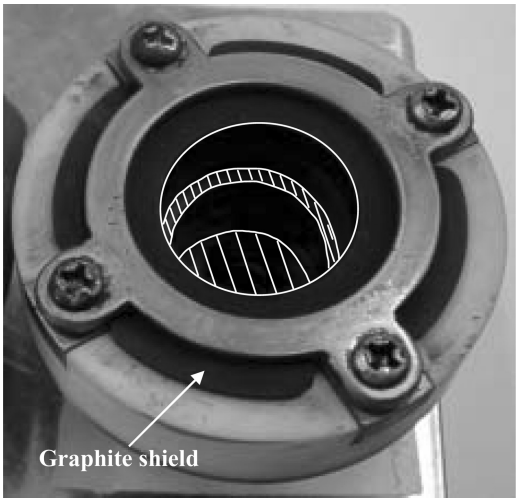

Fig. 7 Graphite shield that protects the magnetic nozzle. White frames are added to highlight the boundaries of the shield. The top shaded area is the boundary between the graphite shield and the ceramic spacer. The bottom shaded area is the upstream surface of the discharge chamber. (The antenna is not shown.)

temperature. Observations in the following section will show that sputtering of the Sm-Co magnet surface was the main factor for the decreases in the magnetic fields. Incidentally, the critical temperature just discussed is different from the Curie temperature at or above which the material loses magnetic force completely. The Curie temperature of Sm-Co magnets is about 750°C.

Although the operation of the microwave engine was unchanged by the reduction in the magnetic field strength, the sputtering damage on the magnetic nozzle surface was significant considering the target lifetime of 5000 h. Therefore, a shield was installed to protect the magnetic nozzle. Graphite was chosen to be the shielding material because of its low sputtering yield. The dimension of the magnetic nozzle and the size of the Sm-Co magnets were modified to install a graphite shield without changing the inner diameter or the magnetic circuit.

IV. 5300-h Endurance Test

After the 1200-h preliminary endurance test, the magnetic nozzle was replaced by a new one that incorporated a graphite shield (see Fig. 7). Also, the filament neutralizer was replaced by a microwave-discharge neutralizer (Fig. 1). The discharge chamber including its antenna from the 1200-h test was used. The microwave engine was disassembled after the 5300-h test, and the masses, dimensions, and magnetic flux densities were measured after each part was cooled down to room temperature.

A. Engine Operation

The microwave engine operation became unstable after nearly 7200 h of operation including the 1200-h test, and the endurance test was stopped. The microwave neutralizer had logged over 5500 h of operation, the magnetic nozzle with a graphite shield had logged over 5200 h of operation, and the other parts of the microwave engine had logged over 7100 h of operation at the end of the endurance test.

Figure 8 shows the acceleration current during the 5300-h endurance test. The microwave engine was operated at the acceleration voltage of 200 V instead of nominal 250 V between 3500th and 5300th hours. This change was made to eliminate flickering of the discharge plasma that started to appear around the 3500th hour. During the flickering, the plasma did not seem to be in any danger of extinguishing. This flickering was different from the instability that led to the end of the tests where the acceleration current started to oscillate between 10 and 43 mA with a period of approximately 2 min. Sputtering yields for Xe on molybdenum (antenna material) and carbon (graphite shield material) decrease by approximately 30% when impacting ion energy is decreased from 250 to

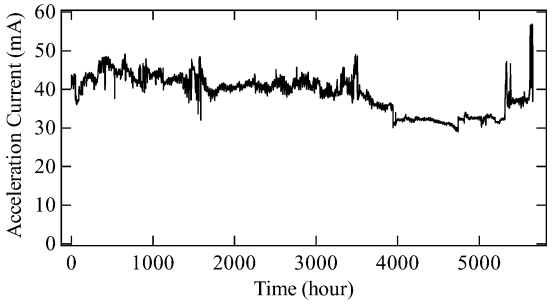

Fig. 8 Acceleration current during the 5300-h endurance test. The microwave engine was operated at the acceleration voltage of 200 V instead of nominal 250 V between 3500th and 5300th hours.

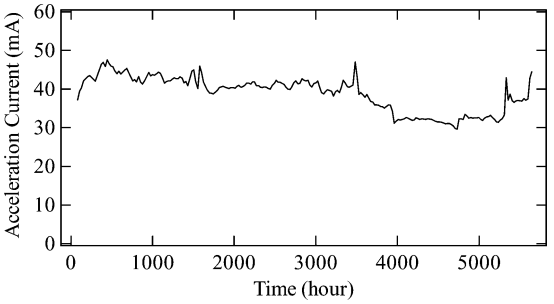

Fig. 9 Averaged acceleration current during the 5300-h endurance test. The data in Fig. 8 were averaged over 24-h periods to cut out the cyclic oscillation in the acceleration current caused by the daily temperature change of the laboratory air.

200 V (Ref. 8). This reduction in sputtering yields can result in the extension of thruster lifetime by roughly 500 h. Sputtering of the graphite shield was probably reduced by more than 30%, because the acceleration voltage reduction also decreased the ion current to the magnetic nozzle surface. On the other hand, sputtering of the discharge chamber magnets and antenna were probably reduced by less than 30%, because the energies of the impacting ions in the discharge chamber were only indirectly influenced by the acceleration voltage. As will be discussed later, the decrease of magnetic field in the discharge chamber was attributed to the end of stable thruster operation, and thus, the impact of the acceleration voltage reduction on the thruster lifetime in this test was thought to be small.

Figure 9 shows acceleration current in the same period as in Fig. 8, but the data were averaged over 24-h periods in order to cut out the cyclic oscillation in the data that were caused by the daily temperature change of the air in the laboratory where the endurance tests were conducted. The thruster performance was affected by the air temperature in the laboratory because the efficiency of the microwave amplifiers, which sat in the room, was temperature dependent. The air temperature in the laboratory varied normally between 21 and 29°C. And correspondingly, the microwave amplifier temperature varied between 23.4 and 30.3°C. For this 6.9°C rise in the amplifier temperature, the forward microwave power decreased by about 3%, which resulted in the reduction of the acceleration current by approximately 1.5% (Ref. 6). These observations were valid only when the amplifier temperature was around 27°C, because the temperature characteristic of the microwave amplifier was not linear. These temperature cycles did not seem to affect the overall thruster operation.

As can be seen in Fig. 9, the acceleration current varied approximately ±5 mA throughout the test, excluding the period where the thruster was operated at 200 V. However, the thruster performance was affected not only by daily room temperature changes but also seasonal changes of the laboratory air. The least change in the air temperature and humidity occurred between 1800th hour and 2500th hour when the air conditioner was turned on in the summer. During this period, the acceleration current varied ±0.6 mA, which corresponds to a thrust variation of ±1.5%.

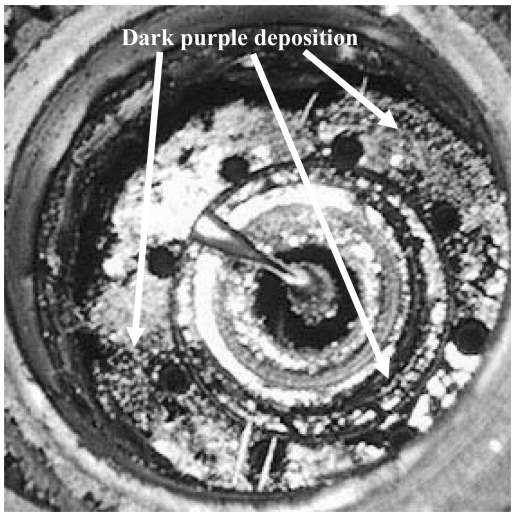

Fig. 10 Discharge chamber after the 5300-h endurance test, after logging over 7100 h of total operation time. Deposition of sputtered material can be seen on all surfaces, which had not been observed in the 1200-h test (see Fig. 5). The L-shaped antenna in the center had been sputtered most at the bend.

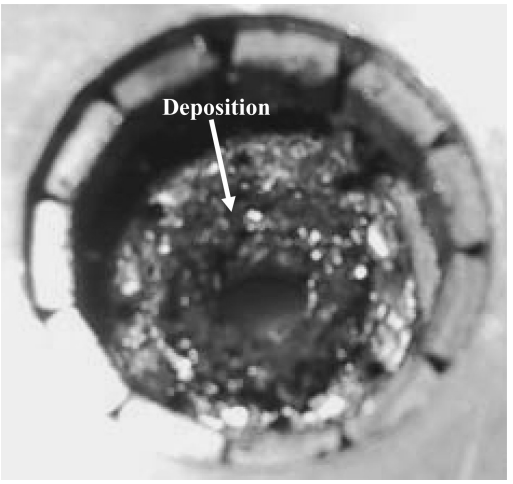

Fig. 11 Neutralizer chamber after the 5300-h endurance test (antenna removed). There was a significant amount of deposition of sputtered Sm-Co, molybdenum, and graphite. The Sm-Co magnets on the inner wall had been shielded from the plasma by an aluminum cylinder (not shown).

B. Discharge Chamber

Figure 10 shows the inside of the discharge chamber after the 5300-h endurance test. The discharge chamber had logged over 7100 h of total operation. There was a dark purple deposition on the lower side of the Sm-Co magnets on the inner wall of the discharge chamber. The same kind of deposition was found on the perimeter of the Sm-Co ring magnet located on the plenum surface, the center of which the antenna came through. This deposition is most likely the sputtered Sm-Co material. The ring magnet was coated with a shiny, silvery deposition that was believed to be sputtered molybdenum from the antenna. The ceramic spacer between the discharge chamber and the magnetic nozzle was covered by graphite and a silvery material (likely molybdenum), but the electrical isolation was maintained until the end of the endurance test.

The mass of the antenna had decreased by 49.2 mg, approximately 1.5% of the original mass, because the beginning of the test. Most of the sputtering of the L-shaped antenna occurred at the bend. The diameter at the antenna tip had decreased from 1.55 to 1.25 mm, while the diameter at the bend had decreased from 1.35 to 0.49 mm in 7100 h of operation. The sputtering pattern follows the magnetic field lines where the lines are converging; most sputtering occurred at the magnetic field cusps. This correlation is also the reason why the Sm-Co magnet surfaces in the inner wall of the discharge chamber were the most sputtered locations in the discharge chamber. It is postulated that sputtering is greatest at the magnetic field cusps because the plasma density is higher there than in other regions in the plasma.

The magnetic flux density of the discharge chamber magnets decreased by 5.0% on average during the 5300-h test. Therefore, the magnetic flux density had decreased by a total of 8.3% in approximately 7100 h of operation. Meanwhile, the magnetic flux density of the ring magnet on the plenum remained constant despite the sputtering and heat ($\sim 60^{\circ}$C). A computer calculation of the magnetic field in the discharge chamber showed that a much stronger magnetic field cusp was formed near the inner wall magnets than near the ring magnet. Therefore, the inner wall magnets were likely to have suffered much more ion impingement than the ring magnet. Another computer calculation showed that the original ECR condition was altered by the decrease of the magnetic flux density in the discharge chamber. The instability in the acceleration current at the end of the endurance test was attributed to this change in the ECR condition. Instabilities in the ion production propagated to the discharge plasma, eventually affecting thruster operation.

C. Magnetic Nozzle

The magnetic nozzle with a graphite shield had logged over 5200 h of operation. At the end of the endurance test, the part of the graphite shield covering Sm-Co magnets had been sputtered through. As in the discharge chamber, most of the sputtering occurred at the magnetic field cusps, near the Sm-Co magnet surfaces. Small holes started to appear on the graphite shield surface at around 4700th hour and had grown in diameter to about between 1 and 2 mm at the end of the endurance test. Because the exposure to the plasma was minimal, the Sm-Co magnets experienced minimum sputtering. And the magnetic flux density of the Sm-Co magnets remained constant during the 5200 h of operation. Most of the sputtered graphite was deposited on the vacuum chamber walls. Some of the sputtered graphite was found on the ceramic spacer and inside the neutralizer chamber. The exit diameter of the graphite shield had increased from 18.93 to 20.50 mm during 5200 h of operation. Recall that the exit diameter of the magnetic nozzle without the graphite shield had increased from 21.00 to 21.70 mm during the first 1200-h endurance test. Therefore, the sputtering was decreased by almost half using graphite shield.

D. Microwave Neutralizer

The microwave neutralizer had logged over 5500 h of operation. There was a significant amount of deposition inside the neutralizer chamber at the end of the endurance test (see Fig. 11). The deposition consisted of sputtered Sm-Co, antenna molybdenum, and graphite. The Sm-Co ring magnet on the plenum had rounded corners caused by sputtering, but the Sm-Co magnets on the inner wall of the neutralizer chamber had no sputtering damage because they were shielded from the plasma by an aluminum cylinder. The L-shaped neutralizer antenna had much more sputtering damage than the discharge chamber antenna. The tip of the antenna had been sputtered away and became needle like. The mass of the antenna had decreased by 154 mg in 5500 h of operation. The mass loss rate was approximately three times as fast as that of the discharge chamber antenna. The diameter at the bend was 0.9 mm, and the diameter at the root was 1.3 mm. The tip of the antenna experienced the greatest erosion because of its proximity to the convergence of the magnetic field lines. The neutralizer orifice, which is made of aluminum, had no sputtering damage. The magnetic flux density of the neutralizer chamber magnets remained constant during the 5500 h of operation caused by the aluminum cylinder shield. The magnetic flux density of the ring magnet also remained constant.

V. Conclusions

A breadboard model of the microwave engine was manufactured, and two endurance tests were performed to verify its durability. After more than 5000 h of operation in the second endurance test, thruster operation became unstable, and the test was stopped. The test has shown that the microwave engine had a lifetime of over 5000 h. The instability in the acceleration current at the end of the endurance test is attributed to the inefficient ECR condition in the discharge chamber that resulted from the decrease in the magnetic flux density of the discharge chamber magnets (8.3% decrease). Instabilities in the ion production propagated to the discharge plasma and eventually led to the adverse effects seen in thruster operation. The magnetic flux density of the magnetic nozzle magnets and neutralizer chamber magnets remained constant because those magnets were physically shielded from the ions. Therefore, a similar shield in the discharge chamber would be expected to protect the chamber magnets. Such a shield would likely require modifications in the chamber dimension and Sm-Co magnet size. After making such modifications, the main life-limiting element in the microwave engine would be the antennas, which are also subjected to ion impingement.

Acknowledgments

The authors wish to thank Takayoshi Kizaki for providing electrical engineering support in the experiments. This work was supported internally by Astro Research Corporation.

References

[1]Chen, F. F., "Waves in Plasmas," *Introduction to Plasma Physics and Controlled Fusion*, 2nd ed., Vol. 1, Plasma Physics, Plenum, New York, 1984, pp. 122–131.

[2]Satori, S., Nagata, A., Okamoto, H., Sugiki, T. M., and Aoki, Y., "New Electrostatic Thruster for Small Satellite Application," AIAA Paper 2000-3275, July 2000.

[3]Satori, S., Okamoto, H., Nakasuka, S., Aoki, Y., and Sugiki, T. M., "Design Status of Engineering Model of Microwave Discharge Electrostatic Thruster," *Proceedings of 3rd International Conference on Spacecraft Propulsion*, Cannes, France, 2000, pp. 467–473.

[4]Satori, S., Okamoto, H., Sugiki, T. M., Aoki, Y., Nagata, A., Itoh, Y., and Kizaki, T., "Development of Microwave Engine," *International Electric Propulsion Conference*, Paper IEPC-01-224, Oct. 2001.

[5]Satori, S., Okamoto, H., Sugiki, T. M., Aoki, Y., Nagata, A., Itoh, Y., and Kizaki, T., "Continuous Operation of Micro Plasma Thruster, Microwave Engine," *Proceedings of the 16th Annual AIAA/USC Conference on Small Satellites*, SSC Paper 02-949, Logan, UT, Aug. 2002.

[6]Kim, S.-W., Satori, S., Itoh, Y., Okamoto, H., Sugiki, T. M., Aoki, Y., Nagata, and Kizaki, T., "Development of Microwave Engine," *International Electric Propulsion Conference*, Paper IEPC-03-251, March 2003.

[7]Kim, S.-W., Itoh, Y., Satori, S., Kizaki, T., Okamoto, H., and Sugiki, "Endurance Test of a 27 W Microwave Engine," AIAA Paper 2003-5014, July 2003.

[8]Rosenberg, D., and Wehner, G. K., "Sputtering Yields for Low-Energy He+-, Kr+-, and Xe+-Ion Bombardment," *Journal of Applied Physics*, Vol. 33, No. 5, 1962, pp. 1842–1845.